J Fluoresc (2011) 21:313–320
DOI 10.1007/s10895-010-0718-x

ORIGINAL PAPER

Synthesis, Characterization, Luminescence and Defect Centres in $CaYAl_3O_7:Eu^{3+}$ Red Phosphor

Vijay Singh · S. Watanabe · T. K. Gundu Rao · Ho-Young Kwak

Received: 16 June 2010 / Accepted: 8 September 2010 / Published online: 1 October 2010

Abstract $CaYAl_3O_7:Eu^{3+}$ phosphor was prepared at furnace temperatures as low as 550°C by a solution combustion method. The formation of crystalline $CaYAl_3O_7:Eu^{3+}$ was confirmed by powder X-Ray diffraction pattern. The prepared phosphor was characterized by SEM, FT-IR and photoluminescence techniques. Photoluminescence measurements indicated that emission spectrum is dominated by the red peak located at 618 nm due to the $^5D_0$–$^7F_2$ electric dipole transition of Eu^{3+} ions. Electron Spin Resonance (ESR) studies were carried out to identify the centres responsible for the thermoluminescence (TL) peaks. Room temperature ESR spectrum of irradiated phosphor appears to be a superposition of two distinct centres. One of the centres (centre I) with principal g-value 2.0126 is identified as an O^- ion while centre II with an isotropic g-factor 2.0060 is assigned to an F^+ centre (singly ionized oxygen vacancy). An additional defect centre is observed during thermal annealing experiments and this centre (assigned to F^+ centre) seems to originate from an F centre (oxygen vacancy with two electrons). The F^+ centre appears to correlate with the observed high temperature TL peak in $CaYAl_3O_7:Eu^{3+}$ phosphor.

Keywords Photoluminescence · Doping · Phosphors · Europium · Combustion · Defect centres · TL

V. Singh (✉) · H.-Y. Kwak (✉)
Mechanical Engineering Department, Chung-Ang University, Seoul 156-756, Korea
e-mail: vijayjiin2006@yahoo.com

H.-Y. Kwak
e-mail: kwakh@cau.ac.kr

S. Watanabe · T. K. G. Rao
Institute of Physics, University of Sao Paulo, 05508-090 Sao Paulo, SP, Brazil

Introduction

Rare-earth ion doped materials with high luminescent efficiencies are in high demand for numerous applications involving the field of electronics, optoelectronics, photonics, biological fluorescence labeling, luminescent paints and many more. Recently, rare-earth activated materials having melilite structure [1–5], a new class of luminescent materials with better physical properties, have attracted significant attention due to their promising photoluminescent properties and potential applications in modern lighting and display fields.

$CaYAl_3O_7$ has the chemical formula of ABC_3O_7, (A = Ca, Sr, Ba; B = La, Gd, Y; C = Al, Ga) belongs to the large families that have melilite structure. In recent years, there are several reports on rare-earth doped ABC_3O_7 compounds [6–9]. Due to the structure features, these compounds have been widely investigated as important optical materials. $LaCaAl_3O_7$ phosphors activated by several ns^2 impurities like Pb^{2+} and Bi^{3+}, and rare-earth dopants were well studied by Kale et al. [10]. Mahakhode et al. [11] reported X-ray-excited luminescence in $GdCaAl_3O_7:Eu^{3+}$. Luminescence of $GdSrGa_3O_7:RE^{3+}$ (RE = Eu, Tb) phosphors and energy transfer from Gd^{3+} to RE^{3+}, have been reported [12]. Bo et al. [13] reported luminescent properties of $LaSrAl_3O_7:RE^{3+}$ (RE = Eu, Tb) prepared by sol-gel method. Kodama et al. [14] reported long-lasting phosphorescence in Ce^{3+}-doped $CaYAl_3O_7$. Later by same group, properties of the phosphorescence and a model of a coupled pair of Ce^{3+} and a defect in the crystals have been reported [15]. Recently, Zhang et al. [16] observed that $CaYAl_3O_7$:Eu phosphor exhibits strong blue mechanoluminescence. It was noticed that many investigations of the synthesis and the crystal chemistry of rare-earth doped melilite families have been reported.

However, a majority of work available on the synthesis of $CaYAl_3O_7$ compounds is generally based on high temperature sintering method. In general, synthesis of the $CaYAl_3O_7$ phase requires high-temperature heat-treatment [14]. It was noticed that there are limited studies on $CaYAl_3O_7$ host though compounds with similar formula and structure have exhibited interesting properties. Moreover, there is a comparative lack of information about the defect properties in this phosphor material. The knowledge about the type of defects, which are dominant in phosphor materials, is very important in order to elucidate information about luminescence process of phosphors and to use them in various applications [17–19]. The defect centres in a material can be detected and studied well using thermoluminescence (TL) and electron spin resonance (ESR) methods.

As per the literature, ESR and TL are among the most useful techniques for investigating the radiation-induced defects and their thermal stabilities in crystalline solids [17–22]. The defect centers created by ionizing radiations, such as alpha, beta and gamma are responsible for thermally stimulated luminescence in the phosphor. In luminescence and defect chemistry, the identification and characterization of the defect centers are essential since defects can play an important role in influencing the electrical, thermal, optical and magnetic properties of the solids. Particularly, the knowledge of defects in the phosphor material is essential in order to understand their thermal stabilities in crystalline solids and luminescence mechanism. During the past few decade, there are several reports [17, 20–25] on the identification of the radiation-induced radicals/defect centers formed on irradiation and the subsequent electron-hole recombination reactions resulting in the TL glow peaks. We have also carried out TL and ESR investigations on gamma-irradiated inorganic phosphors doped with rare-earth ions [26–29].

Solution combustion synthesis is a low temperature synthesis technique that offers a unique synthesis route via a highly exothermic redox reaction between metal nitrates and an organic fuel to produce multi-element oxides. This process offers several advantages like fast heating rates, short reaction time, yields porous and foamy products. It has also the advantages of easily doping desired amounts of dopant ions and low processing temperature. In the present work, we describe the synthesis of Eu^{3+} doped $CaYAl_3O_7$ through combustion route and characterization by powder X-Ray diffraction (PXRD), SEM and FTIR techniques. In addition, this work reports the photoluminescence and TL properties of Eu^{3+} doped $CaYAl_3O_7$ phosphor. ESR studies were also carried out to identify defect centres responsible for TL peaks observed in $CaYAl_3O_7$:Eu^{3+} phosphor.

Experimental

Sample Preparation

$CaYAl_3O_7$:$Eu_{0.03}$ {prepared using [Aluminum nitrate (5 g, $Al(NO_3)_3 \cdot 9H_2O$), Sigma-Aldrich], [Yttrium nitrate (1.7016 g, $Y(NO_3)_3 \cdot 6H_2O$), Sigma-Aldrich], [Calcium nitrate (1.0491 g $Ca(NO_3)_2 \cdot 4H_2O$), Sigma-Aldrich], [Urea (3.1312 g, NH_2CONH_2), Sigma-Aldrich], and [Europium nitrate (0.0570 g, $Eu(NO_3)_3 \cdot 5H_2O$), Sigma-Aldrich]} was prepared by using the solution combustion method. For the combustion, metal nitrates as oxidizers and urea as fuel were used. The oxidizer : fuel ratio was calculated using total oxidizing (O) and reducing valences (F) based on the concept of propellant chemistry [30]. The process involves the exothermic reaction of an oxidizer (metal nitrate) and an organic fuel (urea (NH_2CONH_2)). The energy released due to the exothermic reaction between the metal nitrates and fuel can rapidly heat the system to high temperatures (>1,000°C) without an external heat source. Combustion method, in fact, makes possible the rapid synthesis of several inorganic materials, without the prolonged high temperature treatment of sintering [26–29]. The starting materials were dissolved in a minimum quantity of deionized water in 300 ml capacity china dish. The obtained solution was heated at 80°C on hot plate for about 30 min. The obtained solution is then inserted into a preheated furnace maintained at 550°C. The solution boils-off followed by evolution of large amount of gases, forming fluffy white masses. The combustion was self-sustaining and self-terminated. The entire process lasted for 5–8 min. After combustion, the fluffy product was crushed into a fine powder. This powder was used for further characterization.

Instruments

Powder XRD experiments were performed on a Philips X′ pert X-ray diffractometer with graphite monochromatized CuK_α radiation (λ=0.15418 nm) in the 2θ range from 10° to 80°. PL measurements were performed on a Hitachi F-4500 FL Spectrophotometer. Scanning electron micrographs (SEM) were taken on a Hitachi S-4300 scanning electron microcopy. A ^{60}Co gamma source was used for the irradiation of samples. TL experiments were carried out on a Daybreak 1100 series automated TL reader system with a heating rate of 5°C/Sec in a nitrogen atmosphere. Electron Spin Resonance experiments were carried out using a Bruker EMX ESR spectrometer operating at X-band frequency with 100 kHz modulation frequency. Diphenyl Picryl Hydrazyl (DPPH) was used for calibrating the g-factors of defect centres. Temperature dependence of the ESR spectra was studied using a Bruker B VT 2000 variable temperature accessory.

Results and Discussion

Powder X-Ray Diffraction

Figure 1 shows the PXRD pattern of as-formed $CaYAl_3O_7$:Eu^{3+} powders. Figure illustrates that the as-prepared $CaYAl_3O_7$:Eu^{3+} phosphor was crystalline. It is observed that as-prepared sample has dominant diffraction peaks due to the $CaYAl_3O_7$ (JCPDS, File-26-0135) phase in addition to weak reflex ion (■) lines which might be belonging to reactant or intermediate phases [16, 31–34]. From PXRD pattern, it is clear that sample shows tetragonal symmetry with space group $P\bar{4}2_1m$. It has been reported in the literature that phase-pure $CaYAl_3O_7$ does not exist at lower temperature synthesis process and even after sintering at 1,200°C for 4 h, weak reflections of Y_2O_3 and $Y_4Al_2O_9$ phases were identified. Moreover, the pure tetragonal structure of $CaYAl_3O_7$ was achieved by increasing the sintering temperature to 1,500°C [16]. It is significant that combustion process produce tetragonal structure of $CaYAl_3O_7$ even at furnace temperatures as low as 550°C within a few minutes.

FT-IR

Figure 2 shows the FT-IR spectrum of as-formed $CaYAl_3O_7$:Eu^{3+} powders. Common bands do not exist in spectrum such as the broad O-H band around 3,400 cm^{-1}, the 1,630 cm^{-1} H_2O vibration band, and the bands related to NO_3^- groups at 1,384 cm^{-1}. This should be noted here as these bands were detected very commonly even after sintering the combustion products. However, in the present case impacts of these bands are almost absent. Strong peaks observed in the 400–900 cm^{-1} region are due to several M-O stretching and bending vibrations. Although no sintering was performed, M-O bands could be obtained through the combustion process. These results show that the formation of M-O bands could be formed even at furnace temperatures as low as 550°C, which is several hundred degrees lower than the conventional solid-state reaction.

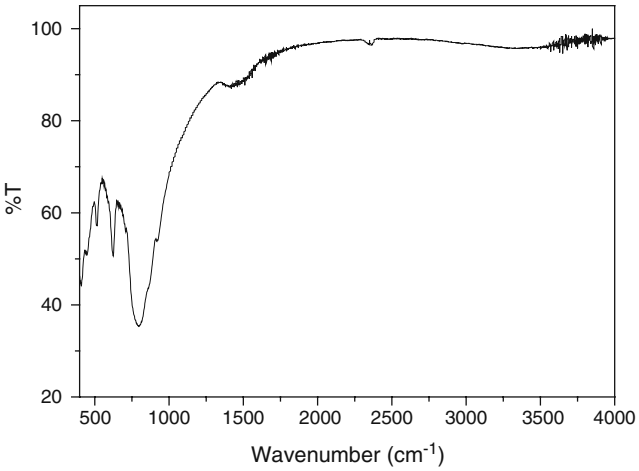

Fig. 2 FT-IR spectrum of as-prepared $CaYAl_3O_7$:Eu^{3+} phosphor

Scanning Electron Microscopy

The SEM micrographs of $CaYAl_3O_7$:Eu^{3+} prepared by the combustion method under various magnifications are shown in Fig. 3. It can be seen from Fig. 3A that the particles of the powder are plate-like crystals with non-uniform shape and size. Due to the uncontrolled dynamics of the process, plate-like crystals are of different shapes and sizes. Surface features of plate-like crystals show that there are several pores. Portion (b) of Fig. 3B is magnified to obtain Fig. 3C. From this SEM micrograph, it is clear that there are presences of several small particles around the pores. We believe that when gas is escaping with high pressure, pores are formed with the simultaneous formation of small particles near the pores. To obtain pore diameter, portion (c) of Fig. 3C is magnified to obtain Fig. 3D. Also portion (d) of Fig. 3D is magnified to obtain Fig. 3E. From Fig. 3E the pore can be measured to have a diameter more than 300 nm. All these features are common in combustion derived products.

Photoluminescence

Figure 4(a) and (b) show photographs of the as-formed $CaYAl_3O_7$:Eu^{3+} powders prepared by the combustion

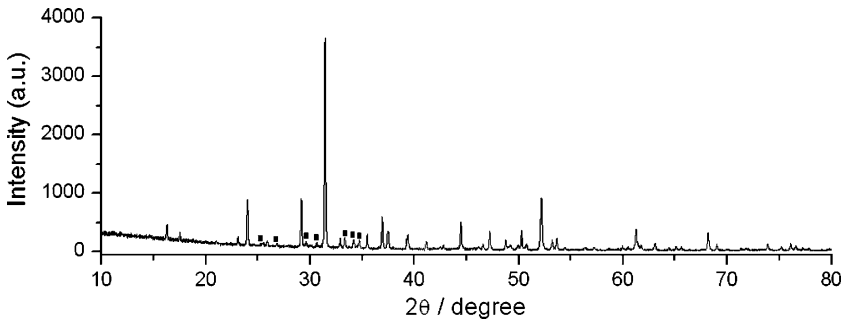

Fig. 1 Powder XRD pattern of as-prepared $CaYAl_3O_7$:Eu^{3+} phosphor

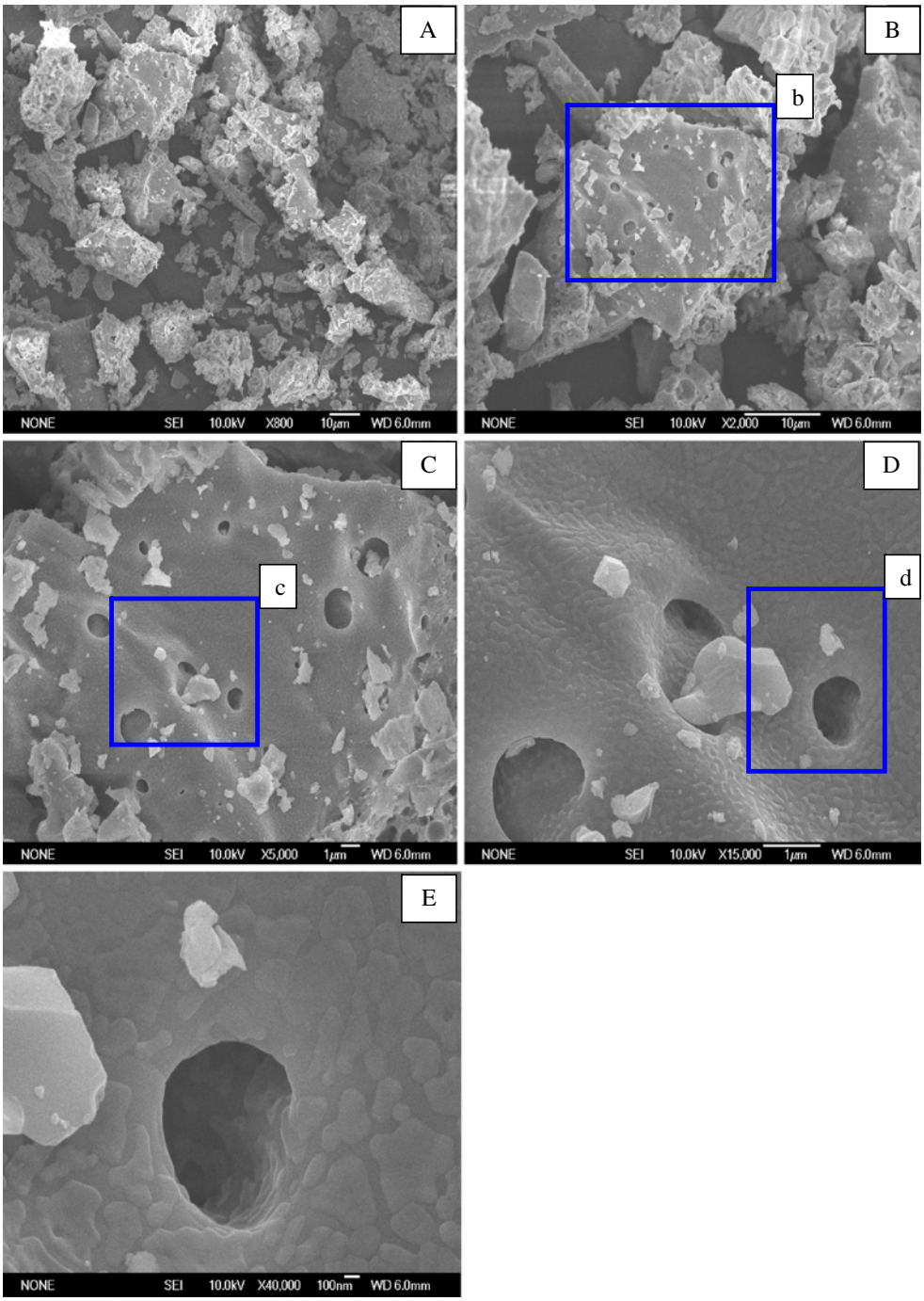

Fig. 3 SEM micrographs of the as-prepared $CaYAl_3O_7:Eu^{3+}$ phosphor

method under room light and UV (254 nm) radiation. Under illumination with ultraviolet light, the white powder fluoresced a uniform bright red color, with no dark patches. Figure 5 shows the excitation (a) and emission (b) spectra of $CaYAl_3O_7:Eu^{3+}$ powder phosphor. The excitation spectrum (Fig. 5a) consists of a broad band and some sharp lines. The broad band is due to part of the charge transfer band (CTB) of Eu^{3+}-O^{2-} bond, and sharp lines are from the f-f transitions within Eu^{3+} $4f^6$ electron configuration. It should be noted here that the position of the CTB band at 254 nm is suitable for Hg discharge-based lamp applications. The excitation peak at 396 nm and 466 nm can also be seen which are attributed to the $^7F_0$–$^5L_6$ and $^7F_0$–$^5D_2$ transitions of Eu^{3+} respectively in addition to many other weak lines due to the various f–f transitions of Eu^{3+}. Figure 5(b) shows the emission spectra of the $CaYAl_3O_7:Eu^{3+}$ phosphor that is measured as a function of different excitation wavelengths observed in the excitation profile of Fig. 5(a). It can be seen from Fig. 5(b) that the spectrum is dominated by the main lines at 618 nm due to the $^5D_0$–$^7F_2$ transition and 590 nm due to the $^5D_0$–$^7F_1$ transition. The peaks from $^5D_0$ to $^7F_2$ (electric-dipole transition) is stronger

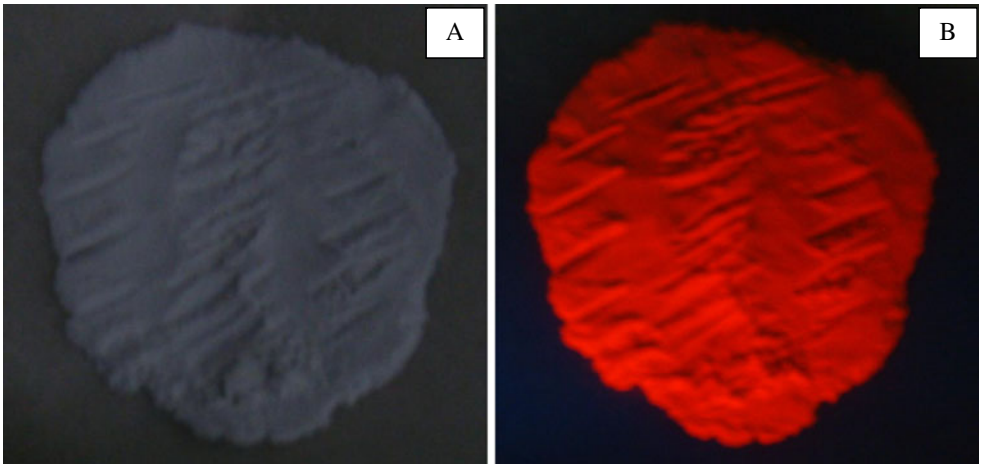

Fig. 4 Typical photographs of an as-prepared $CaYAl_3O_7:Eu^{3+}$ phosphor sample under **a** room light (appearance: a white powder) and **b** UV-254 nm (appearance: strong red emission of $^5D_0$–$^7F_2$ transition of Eu^{3+})

than that from $^5D_0$ to $^7F_1$ (magnetic-dipole transition), which indicates that Eu^{3+} occupies the Y^{3+} site with no inversion symmetry. On the other hand, Eu^{3+} ions may easily incorporated into the Y^{3+} sites due to the similar radius [16]. We have also observed, on varying the excitation wavelength, that there are no significant changes in the emission spectra except for their higher emission intensity, which seem to indicate that europium is incorporated in exclusively trivalent form at Y^{3+} sites.

TL and ESR

Figure 6 shows a typical TL glow curve for $CaYAl_3O_7:Eu^{3+}$ phosphor at a test gamma dose of 5 Gy. The main TL glow peak occurs at about 470°C with a minor peak at 190°C. The glow curve has been recorded at a heating rate of 5°C/Sec.

The ESR spectrum at room temperature (dose: 10 kGy) of Eu^{3+} doped $CaYAl_3O_7$ is shown in Fig. 7. The observed spectrum is a superposition of at least two defect centres. This inference is based on thermal annealing experiments. It is possible to identify two centres and these are labeled in Fig. 7. The ESR lines labeled as I is due to a centre characterized by an isotropic g-value equal to 2.0126. Centre I exhibits several resonance lines and these lines are not clearly resolved. About nine lines are seen and some of the other lines are overlapped by the ESR line of an another centre. In $CaYAl_3O_7$ aluminum (^{27}Al), calcium (^{43}Ca) as well as yttrium (^{89}Y) have isotopes with nuclear spin. ^{27}Al has a nuclear spin 5/2 (magnetic moment: 3.6415) with 100% abundance. On the other hand, ^{43}Ca (nuclear spin 7/2 and magnetic moment: 1.3173) has an abundance of 0.14% whilst ^{89}Y (nuclear spin 1/2 and magnetic moment: 0.1374) has an abundance of 100% [35]. Therefore, the possibility of the electronic spin interacting with aluminum (^{27}Al) and yttrium (^{89}Y) ions is more due to the ions larger abundance. The observed lines are presumably due to hyperfine interaction with two equivalent nuclei of neighbouring Al^{3+} ions as a consequence of the larger magnetic moment of the ion. Interaction with yttrium ions is likely to give rise to a small broadening of the resonance line as the corresponding magnetic moment is small.

$CaYAl_3O_7$ has the melilite structure (a tetragonal sheet structure) with space group $P\bar{4}2_1m$. The Ca^{2+}/ Y^{3+} ions are randomly distributed on their common lattice sites. There is a possibility of mixed occupancy in the Al site, with partial replacement by Ca/Y atoms. Consequently, a number of

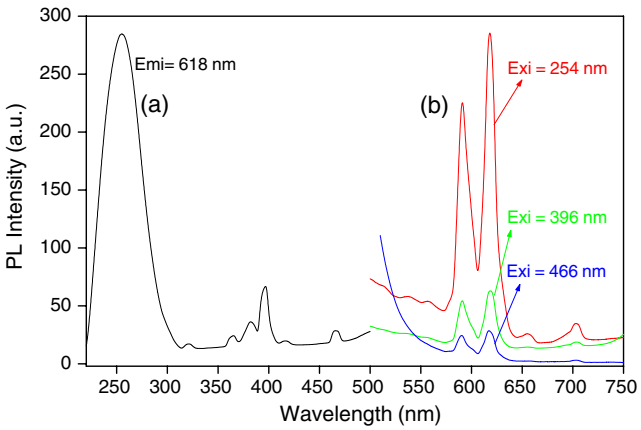

Fig. 5 Photoluminescence spectra of the as-prepared $CaYAl_3O_7:Eu^{3+}$ phosphor **a** Excitation spectrum and **b** Emission spectrum

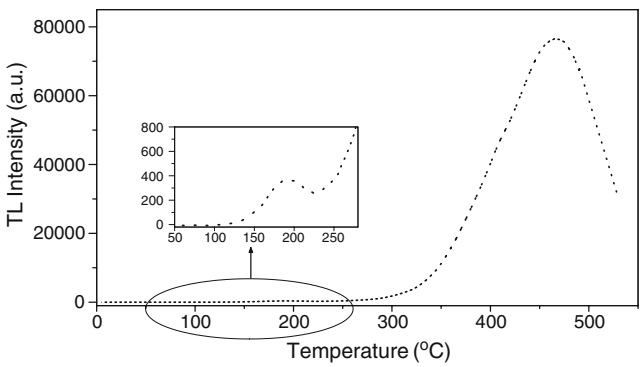

Fig. 6 TL glow curve of $CaYAl_3O_7:Eu^{3+}$ phosphor (test gamma dose: 5 Gy)

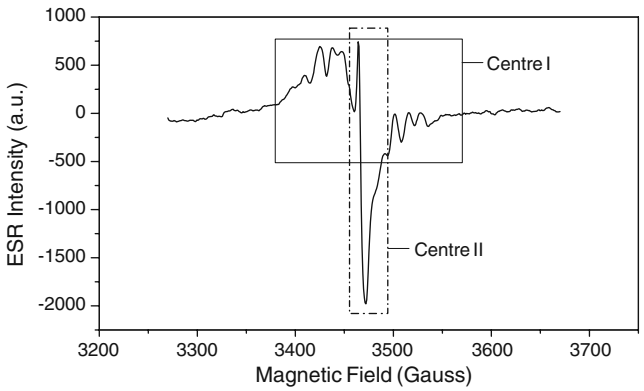

Fig. 7 Room temperature ESR spectra of irradiated $CaYAl_3O_7:Eu^{3+}$ phosphor (gamma dose: 10 kGy). Line labeled as I is due to an O^- ion. Centre II line is assigned to a F^+ centre

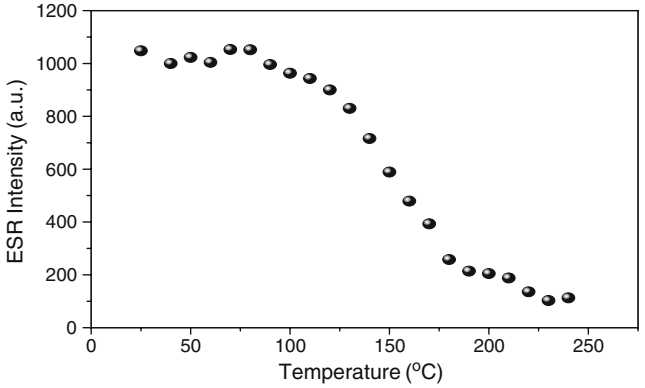

Fig. 8 Thermal annealing behaviour of centre I (O^- ion) in $CaYAl_3O_7:Eu^{3+}$ phosphor

trapping sites for the electron and hole on irradiation are created due to antisite formation which results from the interchange of the ions on tetrahedral and rectangular anti-prism lattice positions by divalent and trivalent ions. Furthermore, a change in the charge state of defect centres and impurities in the lattice is possible due to damage created by irradiation [36]. These defect centres play an important role in many of the luminescent and optical properties of the crystal.

Non-stoichiometry and the above mentioned cation disorder of $CaYAl_3O_7$ provide a large number of lattice defects, which may serve as trapping centres. In such a case, after irradiation, oxygen vacancies should lead to F^+-centers by trapping electrons. Furthermore, O^- ions can be formed by hole trapping at calcium, yttrium or aluminum vacancies. The observed hyperfine lines of centre I indicates that the unpaired electron is delocalized and interacts with nearby aluminum nuclei. Hence centre I is assigned to an O^- centre stabilized by a nearby cation vacancy (a hole trapped in a $Ca^{2+}/Y^{3+}/Al^{3+}$ ion vacancy).

A pulsed-thermal annealing method was used to measure the stability of centre I. After heating the sample up to a given temperature, where it is maintained for 3 min, it is cooled rapidly down to room temperature for ESR measurements. Figure 8 shows the thermal annealing behaviour of centre I. It is seen that the centre becomes unstable around 100°C and decays in the temperature range 100°C–240°C. This decay appears to relate to the TL peak at 190°C.

Centre II in Fig. 7 is characterized by an isotropic g-value equal to 2.0060 and 5 gauss linewidth. A probable centre which can be formed after irradiation in this phosphor is an F^+ center (an electron trapped at an anion vacancy). The first observation of such a centre was in neutron irradiated LiF [37] where the centre exhibited a broad ESR line (linewidth ~ 100 gauss). It may be mentioned that the F^+ centre inherently has a narrow linewidth of about 1 gauss (as observed in MgO system [38]). The observed linewidth depends on the ions present in the system (whether they have nuclei with magnetic moment and their abundance) and also on the amount of delocalization of the unpaired electron which depends on the host lattice. F^+ centres are characterized by a small g-shift, which may be positive or negative, a linewidth which depends on the host lattice. The trapping of an electron at an anionic vacancy forms the basis for formation of F^+ centres. Hyperfine interaction with the nearest-neighbor cations is the major contribution to the linewidth. Defect centre II formed in the present system is characterized by a small g-shift. The centre does not exhibit hyperfine structure. Recently, such a centre was reported in aluminate systems like $LiAlO_2$ and $ZnAl_2O_4$ phosphors [39, 40]. On the basis of these observations, centre II is tentatively assigned to an F^+ centre.

Figure 9 shows the thermal annealing behaviour of centre II. It is observed that the centre becomes unstable near 90°C and decays in the temperature range 90°C–270°C. Centre II also appears to be associated with the TL peak at 190°C. It is to be noted that there is a close similarity

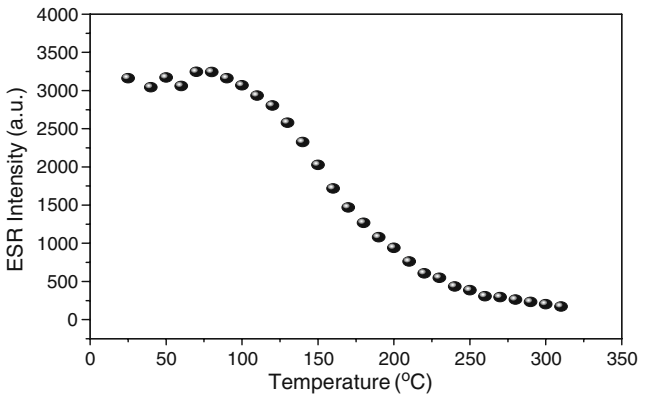

Fig. 9 Thermal annealing behaviour of centre II (F^+ centre) in $CaYAl_3O_7:Eu^{3+}$ phosphor

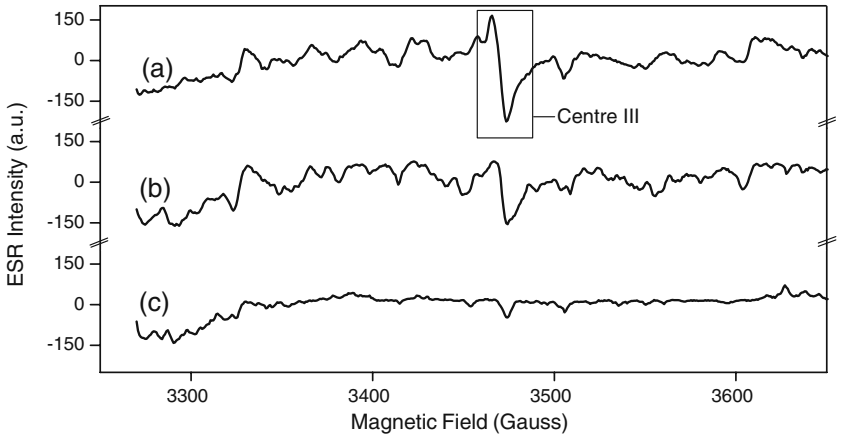

Fig. 10 Room temperature ESR spectrum of irradiated $CaYAl_3O_7:Eu^{3+}$ phosphor (gamma dose : 10 kGy) after thermal anneal at (**a**) 360°C, (**b**) 450°C and (**c**) 520°C. Centre III line is assigned to a F^+ centre

between the decays of centres I and II. This indicates that centre II may be acting as a recombination centre when the hole from O^- ion (centre I) is released and recombines with the electron in F^+ centre.

The two centres observed in irradiated $CaYAl_3O_7:Eu^{3+}$ are found to decay below 300°C. A careful examination of the ESR spectra during high temperature thermal annealing has shown a new centre (Centre III). The observed ESR spectrum after thermal anneal at 360°C is shown in Fig. 10. The intensity of the ESR line is found to be relatively small. Centre III has an isotropic g-factor equal to 2.0039 with a eight gauss linewidth and is tentatively assigned to a F^+-centre based on the reasons mentioned earlier. It may be mentioned that the E_1'centre (an oxygen vacancy having an unpaired electron localized in the sp^3 hybrid orbital extending into the vacancy from the adjacent silicon ion) in SiO_2 exhibits a similar formation behaviour as centre III. Jani et al. [41] have investigated in detail the formation and thermal annealing characteristics of E_1' centre in SiO_2. They have proposed an oxygen vacancy containing two electrons in a singlet state (S=0) as the precursor of the E_1' centre. They suggest that this oxygen vacancy with two electrons is likely to release an electron during post-irradiation heating resulting in the formation of E_1' centre. On the basis of these results in SiO_2, it is speculated that in $CaYAl_3O_7:Eu^{3+}$ phosphor the formation process of centre III might be similar.

Room temperature irradiation can convert oxygen vacancies, which are present in $CaYAl_3O_7$ lattice due to non-stoichimetry and impurities, into F-centres. F-centre contains two electrons in a singlet state (S=0) and during heating releases an electron which appears in the thermal annealing experiments as an appearance of centre III. The thermal annealing behaviour of centre III is shown in Fig. 11. It is seen that the centre decays in the temperature region 400°C–500°C. The present results indicate that centre III correlates with the 470°C TL peak in the phosphor.

Conclusions

Red phosphor $CaYAl_3O_7:Eu^{3+}$ could be prepared by a simple, fast and economical viable combustion method. PL investigations show the strongest emission at 618 nm corresponding to the electric dipole $^5D_0$–$^7F_2$ transition of Eu^{3+} in $CaYAl_3O_7$ due to the non-centrosymmetric nature of the Eu^{3+} ion site, which results in pure red color emitting. $CaYAl_3O_7:Eu^{3+}$ phosphor exhibits TL glow peaks at 190°C and 470°C. Three defect centres have been identified in the irradiated phosphor. These centres are tentatively assigned to an O^- ion and F^+ centres. O^- ion correlates with the 190°C TL peak. One of the F^+ centres appears to act as a recombination centre for the peak at 190°C. The F^+ centre seen after high

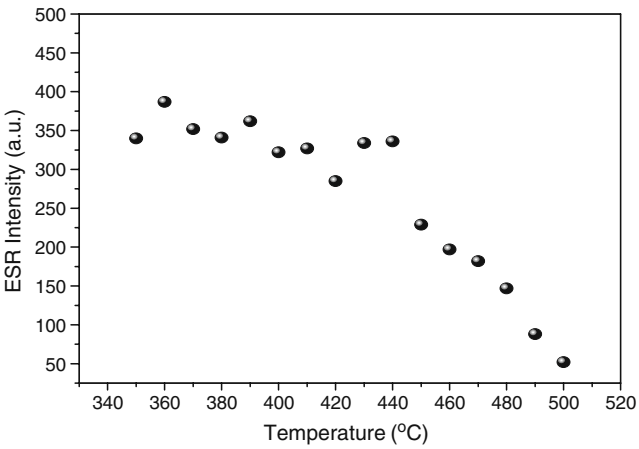

Fig. 11 Thermal annealing behaviour of centre III (F^+ centre) in $CaYAl_3O_7:Eu^{3+}$ phosphor

temperature anneal appears to correlate with the TL peak at 470°C.

Acknowledgments Dr. Vijay Singh expresses his thanks to the Chung-Ang University, Seoul (South Korea) for providing the Research Assistant Professorship. T. K. Gundu Rao is grateful to FAPESP, Brazil for the research fellowship.

References

1. Raj ES, Skinner SJ, Kilner JA (2005) Solid State Ion 176:1097
2. Kaczkan M, Pracka I, Malinowski M (2004) Opt Mater 25:345
3. Wang XJ, Jia D, Yen WM (2003) J Lumin 102–103:34
4. Yamaga M, Tanii Y, Kodama N, Takahashi T, Honda M (2002) Phys Rev B 65:235108
5. Malinowski M, Pracka I, Myziak P, Piramidowicz R, Wolinski W (1997) J Lumin 72–74:224
6. Kodama N, Takahashi T, Yamaga M, Tanii Y, Qiu J, Hirao K (1999) Appl Phys Lett 75:1715
7. Kodama N, Sasaki N, Yamaga M, Masu Y (2001) J Lumin 94–95:19
8. Zhou L, Choy WCH, Shi JX (2005) J Solid State Chem 178:3004
9. Wang YH, Wang DY (2006) J Electrochem Soc 153:H166
10. Kale MA, Joshi CP, Moharil SV, Muthal PL, Dhopte SM (2008) J Lumin 128:1225
11. Mahakhode JG, Dhoble SJ, Joshi CP, Moharil SV (2007) J Alloys Compd 438:293
12. Zhang X, Zhang J, Liang L, Su Q (2005) Mater Res Bull 40:281
13. Bao A, Tao C, Yang H (2008) J Mater Sci Mater Electron 19:476
14. Kodama N, Takahashi T, Yamaga M, Tanii Y, Qiu J, Hirao K (1999) Appl Phys Lett 75:1715
15. Kodama N, Tanii Y, Yamaga M (2000) J Lumin 87–89:1076
16. Zhang H, Yamada H, Terasaki N, Xu CN (2008) J Electrochem Soc 155(5):J128
17. Gundu Rao TK, Bhatt BC, Shrivastava JK, Nambi KSV (1993) J Phys Condens Matter 5:1791
18. Lempicki A, Bartram R (1999) J Lumin 81:13
19. Nikl M, Mihokova E, Pejchal J, Vedda A, Zorenko Y, Nejezchleb K (2005) Phys Status Solidi B 242:R119
20. Gundu Rao TK, Shinde SS, Bhatt BC, Shrivastava JK, Nambi KSV (1995) J Phys Condens Matter 7:6569
21. Shinde SS, Gundu Rao TK, Sanaye SS, Bhatt BC (1999) Radiat Prot Dosim 84:215
22. Murali S, Natarajan V, Venkataramani R, Pushparaja, Sastry MD (2001) Appl Radiat Isot 55:253
23. Murali S, Natarajan V, Seshagiri TK, Kadam RM, Venkataramani R, Sastry MD (2003) Radiat Meas 37:259
24. Dhoble SJ, Moharil SV, Gundu Rao TK (2007) J Lumin 126:383
25. Gundurao Rao TK, Moharil SV (2007) Radiat Meas 42:35
26. Singh V, Gundu Rao TK (2008) J Solid State Chem 181:1387
27. Singh V, Watanabe S, Gundu Rao TK, Chubaci JFD, Ledoux-Rak I, Kwak HY (2010) Appl Phys B Lasers Opt 98:165
28. Singh V, Rai VK, Ledoux-Rak I, Watanabe S, Gundu Rao TK, Chubaci JFD, Badie L, Pelle F, Ivanova S (2009) J Phys D Appl Phys 42:065104
29. Singh V, Gundu Rao TK, Zhu JJ (2008) J Lumin 128:583
30. Jain SR, Adiga KC, Pai Vernekar VR (1981) Combust Flame 40:71
31. Fu R, Chen K, Agathopoulos S, Ferro MC, Tulyaganov DU, Ferreira JMF (2005) J Mater Sci 40:2425
32. Qiao L, Zhou H, Xue H, Wang S (2003) J Eur Ceram Soc 23:61
33. Liu Y, Zhou H, Qiao L, Wu Y (1999) J Mater Sci Lett 18:703
34. Jackson TB, Virkar AV, More KL, Dinwideie RB, Cutler RA (1997) J Am Ceram Soc 80:1421
35. Handbook of Chemistry and Physics, edited by R. C. Weast. CRC, Cleveland, (1971)
36. Summers GP, White GS, Lee KH, Crawford JH (1980) Phys Rev B21:2578
37. Hutchison CA (1949) Phys Rev 75:1769
38. Wertz JE, Auzins P, Weeks RA, Silsbee RH (1957) Phys Rev 107:1535
39. Dhabekar B, Alagu Raja E, Menon S, Gundu Rao TK, Kher RK, Bhatt BC (2008) Rad Meas 43:291
40. Menon S, Dhabekar B, Alagu Raja E, More SP, Gundu Rao TK, Kher RK (2008) J Lumin 128:1673
41. Jani MG, Bossoli RB, Halliburton LE (1983) Phys Rev B27:2285